

Promotion of Neuronal Guidance Growth by Aminated Graphene Oxide via Netrin-1/Deleted in Colorectal Cancer Signaling

Meili Liu, Chongquan Huang, Zhengtai Jia, Zhijun Zhao, Xiongfuxiao, Anqing Wang, Ping Li, Xiali Guan, Gang Zhou,* and Yubo Fan*



Cite This: *ACS Chem. Neurosci.* 2020, 11, 604–614



Read Online

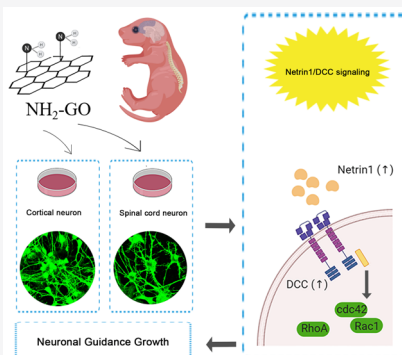
ACCESS |

Metrics & More

Article Recommendations

ABSTRACT: Promotion of neurite outgrowth and synapse formation is a key step for nervous tissue regeneration. It is important for finding a new biomaterial to guide neuron growth to target neurons. Aminated graphene oxide ($\text{NH}_2\text{-GO}$) displays electrical properties and dispersibility, which may change the surface charge of neurons and further activate neuronal excitement. However, the molecular guidance mechanism of $\text{NH}_2\text{-GO}$ on neurite outgrowth is seldom reported. In this study, we compared the role of $\text{NH}_2\text{-GO}$ on the spinal cord neurons and cortical neurons. Results indicated that the proper concentrations were at 2 and 4 $\mu\text{g}/\text{mL}$ as determined by the CCK-8 assay. Notably, $\text{NH}_2\text{-GO}$ (2 and 4 $\mu\text{g}/\text{mL}$) improved the dispersibility and strengthened the effect of the composite material. In addition, it enables biocompatibility and efficient guidance of growth performance, which is not neurotoxic for neuronal outgrowth under these two concentrations. More interestingly, $\text{NH}_2\text{-GO}$ at 2 $\mu\text{g}/\text{mL}$ induced both marked neurite elongation and increased branches in cortical neurons, but there is no significant change of neurite length and branches in spinal cord neurons. Further, the fluorescence intensity and mRNA level of Netrin-1 and DCC (Deleted in Colorectal Cancer) were both enhanced by $\text{NH}_2\text{-GO}$ at 2 $\mu\text{g}/\text{mL}$. Moreover, the function of Netrin-1 and DCC were activated more significantly by $\text{NH}_2\text{-GO}$ at 2 $\mu\text{g}/\text{mL}$ in cortical neurons than that of spinal cord neurons. When RhoA was inhibited by the C3 exoenzyme, phosphorylated Rac1 and Cdc42 expression decreased significantly. Thus, $\text{NH}_2\text{-GO}$ at 2 $\mu\text{g}/\text{mL}$ could influence Netrin-1/DCC signaling and the downstream RhoGTPase pathway, which may be preferred to guide the neurite growth in cortical neurons. It will provide a promising approach for the development of novel therapeutic methods of nerve regeneration.

KEYWORDS: aminated graphene, neurite outgrowth, netrin-1, DCC, RhoGTPase, nerve regeneration



1. INTRODUCTION

Numerous patients have suffered from various neurological diseases including intracranial injury (TBI), spinal cord injury (SCI), and neurodegeneration. Many engineering methods have been reported to have progress in treatment, including guiding axons of neurons, the generation of multiple types of neurons, reconstruction of the neural circuit, and stem cell transplantation.^{1–3} However, regenerative neurons often grow slowly with no connection with target neurons, which often influences synapse formation after the methods are employed. Thus, an approach to promoting axonal guidance growth in regenerative medicine needs to be developed. Accurate control of axon guidance and synaptic junction formation play a key role on repairing or mimicking neural network.⁴ Neurite outgrowth was strongly limited by a wrong axonal connection.⁵

Researchers have found that graphene oxide (GO), which is derived from graphene, have received a particular focus because of its oxygen functional groups ($-\text{OH}$, $\text{O}=\text{C}-\text{O}$).⁶ Matrix membranes mixed with aminated graphene oxide can improve hydrophilicity, osmolarity, and stain resistance

because of its higher porosity and finer pores modified by polar groups on the surface of aminated graphene oxide nanosheets.⁷ Interestingly, graphene (G) or graphene oxide (GO) was considered to have distinguishing features to affect neuron behaviors such as cell growth, adhesion, differentiation, and migration.^{8–11} Additionally, G or GO can enhance the neurogenesis of neural stem cells (NSCs) by inducing specific directional alignment of neurons.¹¹ Patterns of graphene derivatives can be potentially used to mediate adhesion, alignment, and synaptic formation.⁴ However, studies on graphene applied on primary cultured neurons are rarely reported.

Various derivatives of graphene in regenerative medicine have been identified. GO sheets or GO nanomaterials with

Received: November 21, 2019

Accepted: January 24, 2020

Published: January 24, 2020

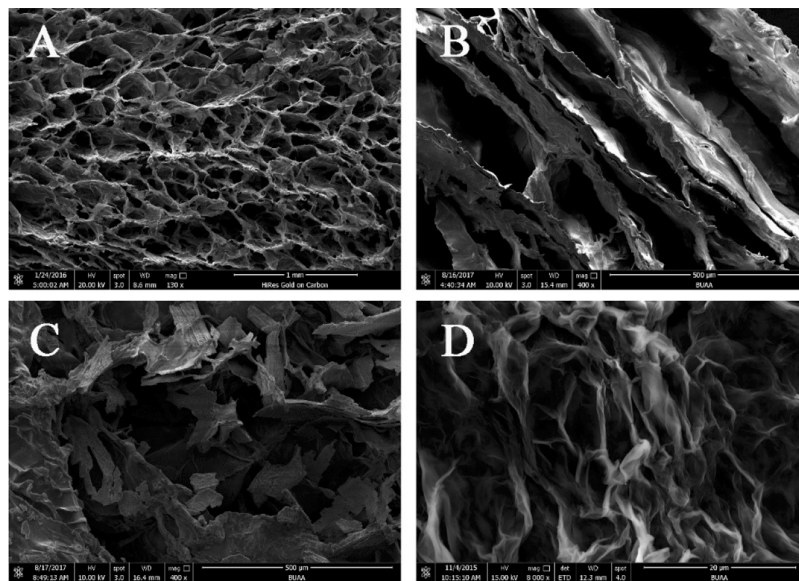


Figure 1. SEM of NH₂-GO composite. (A) The sectional view (130×). (B) The sectional view (400×). (C) The surface view (400×). (D) The internal view (8000×).

different functional groups have been used to improve neuronal growths and repair injured neurons. Functionalization and dispersion can maintain the natural properties of graphene. Previous researchers have concentrated on a single modification method especially in carboxylation, while fewer researchers are concerned about the differences of those modification methods, such as the mechanism of detoxification performance and the molecular mechanism on tissue engineering.^{6,12} Meanwhile, amination means easily formed hydrogen bonding and electrostatic interactions between adsorbed target and animated groups depend on their charge capacity. GO can be modified into aminated graphene oxide (NH₂-GO). GO functionalization with an aminated group has gained importance because it has positive charges and promotes the formation of hydrogen bonds between neurons and nanomaterials.¹³ However, the molecular mechanism of NH₂-GO on axonal growth remains unclear.

The amination modification of graphene is considered one of the most effective modification methods. An added amino group on the surface can improve the hydrophobicity and polarity of the graphene, thereby enhancing its dispersibility in the polymer and forming a hydrogen bond or a chemical bond between the graphene and the polymer. After binding to the cation, the graphene can be cross-linked with DNA, thereby serving as a carrier material for the transfected gene.¹⁴ In the field of neuronal study, graphene can be used as a material for nerve interfaces, owing to its good electrical conductivity and biocompatibility.¹⁵ Meanwhile, graphene promotes not only the growth of peripheral neurons¹⁶ but also the differentiation of neural stem cells into the nerve direction and inhibits their differentiation into glial cells.⁸ Convertino et al. fabricated graphene on the SiC surface and treated it with type I collagen, PLL, PDL, and so on and cultured PC12 cells and DRG cells. The DRG neurons showed a higher survival rate and a stronger network, and the PC12 cells showed a longer neurite outgrowth and higher differentiation efficiency.¹⁶ Park et al. compared the hNSCs cultured on glass and graphene; the cells exhibited neuronal differentiation stability, and graphene showed good electrical coupling with differentiated neural

cells.⁸ However, research on improving the properties of graphene itself remains mainly focused on the primary aspects, such as materials and cytotoxicity. Studies concerning the biological effects of the functional group of graphene on neurons are rarely reported.

Previous studies were mainly focused on the corresponding synapse formation in nerve regeneration. Notably, formation of the synapse is critical in the complex neuronal network system.¹⁷ During nervous system development, growth cones guide axons to target neurons. However, growth cones often produce some attraction or repulsion signals.¹⁸ Netrin-1 can mediate the cellular migration and outgrowth,^{19,20} which can bind different receptor to induce axon attraction or repulsion.^{21–23} Moreover, Netrin-1 guides injured axon growth to the distal nerve stump in rat sciatic nerve.²⁴ However, studies rarely focus on the involvement of Netrin-1 in the nanomaterial (particularly aminated graphene oxide, NH₂-GO) repair of injured neurons. Our recent study indicated that graphene can influence growth of neurons by triggering the Netrin-1/DCC (Deleted in Colorectal Cancer) pathway.²⁵ However, graphene as a different type can cause neurotoxicity in neuronal growth to a certain degree. The role of NH₂-GO in guiding the neuronal growth needs to be investigated.

Here, we reported the role of NH₂-GO on neurite outgrowth. NH₂-GO can efficiently activate Netrin-1/DCC signaling to mediate neuronal growth. These studies can provide a useful method for nerve tissue engineering.

2. RESULTS AND DISCUSSION

2.1. SEM Observation. Neuronal functional regeneration is very difficult, which is often related to the failure of axonal connection. Graphene was popular as nanomaterial because of its great physicochemical properties of hybrid structures and biocompatibility.¹¹ A previous study indicated that GO can be used as nanoscaffolds for regenerating injured spinal cord axons *in vivo*.²⁶ However, GO cannot efficiently repair impaired communication in neurons. Thus, it is important to develop a novel graphene that can specifically control the axonal connection and growth of regenerative neurons after

nerve injury. Amination enables easily formed hydrogen bonding and electrostatic interactions between adsorbed target and aminated groups depending on their charge capacity. Thus, we developed aminated graphene oxide ($\text{NH}_2\text{-GO}$) to guide axonal growth in this study.

The microstructure of $\text{NH}_2\text{-GO}$ composite is shown in Figure 1. As shown in Figure 1a), the typical porous network structure could lead to an increase in specific surface area and active functional groups in the structure. It enables the biocompatibility and efficient guidance growth performance. Figure 1b,c proves the existence of continuous porous structures on a three-dimensional scale, which implies benefit for cell growth in space. Figure 1d shows that the porous structure of $\text{NH}_2\text{-GO}$ could remain in very small size. Free-standing $\text{NH}_2\text{-GO}$ nanosheets with typical wrinkles appear, and the composite presents a generally smooth morphology.

2.2. Raman Spectroscopy Analysis. The Raman spectrum of GO and the as-prepared $\text{NH}_2\text{-GO}$ composite is presented in Figure 2. The D and G peaks were observed in

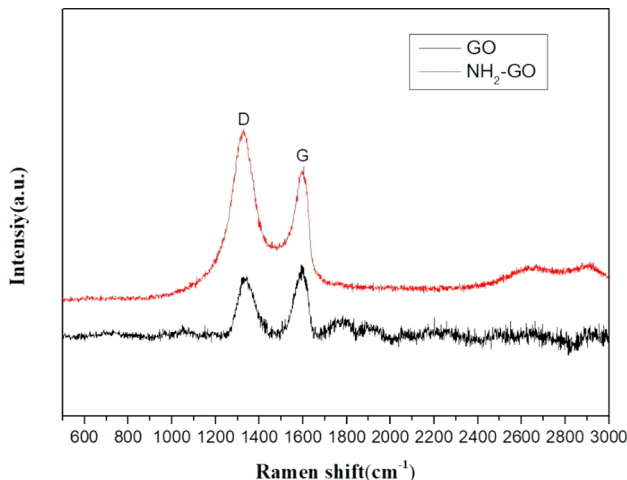


Figure 2. Raman shift curve of $\text{NH}_2\text{-GO}$ and GO.

both curves. The intensity of D peaks was related to the density of the side chain groups. The intensity ratio of the D peak to G peak (ID/IG) was related to the structural defect. From Figure 2, The D peak of $\text{NH}_2\text{-GO}$ was stronger than GO and the ID/IG was larger, which implied more defect and new groups in the carbon chain. Obviously, the D peak at 1420 cm^{-1} was ascribed to the stretching vibrations of the C=O of carboxyl group. The peaks 1690 cm^{-1} was ascribed to the C=C group of the aromatic ring. The larger ID/IG of $\text{NH}_2\text{-GO}$ was corresponded to the C=O group of amide linkages, N—H of amide band and C—N stretch of amide, which indicated that the ethidene diamine compounds were successfully coupled to the edge of GO surface.

2.3. Thermal Analysis. The result of thermal analysis is presented in Figure 3. The red curve is the result of thermogravimetric analysis (TG), and the blue one is the result of the differential thermal analysis (DTA). The black curves are the TG and DTA results of GO.

Around $170\text{ }^\circ\text{C}$ for $\text{NH}_2\text{-GO}$, the TG curve showed a linear decline with a slope close to -1 , and the DTA curve had a sharp endothermic peak at the same temperature, indicating that $\text{NH}_2\text{-GO}$ had a severe dehydration reaction at this temperature. TG and DTA results of GO was similar except that the temperature was $150\text{ }^\circ\text{C}$. The similar trend of those

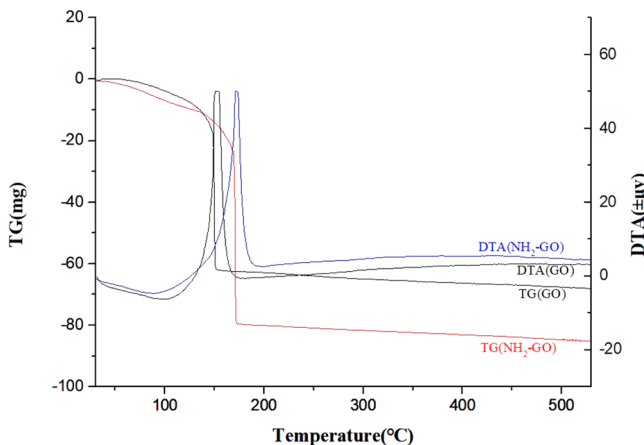


Figure 3. Thermal analysis curves of $\text{NH}_2\text{-GO}$ and GO.

curves implied that $\text{NH}_2\text{-GO}$ has the similar basic structure and elementals as GO. However, the existence of extra N-containing groups in $\text{NH}_2\text{-GO}$ delayed the occurrence of severe dehydration reactions, and less composite remained after the reaction. The result is consistent with the Raman spectrum.

2.4. Adsorption Performance. $\text{NH}_2\text{-GO}$ is modified from GO, which is rich in positively charged groups. In addition, it can adsorb many kinds of proteins, which possibly impacts the nerve conduction. The adsorption equilibrium of both composites was achieved within 1 h, which was much shorter than other adsorbents reported. No significant difference in speed of arrival of adsorption equilibrium was found. Both composites were supposed to be high reactivity, dispersibility, and stability. The active groups could serve as adsorption sites for adsorbed target. However, the degree of adsorption of amination is significantly higher than that of carboxylate graphene oxide as shown in Figure 4A, which can be explained by its positive charge facilitating protein adsorption. This electrical signal can activate neuronal excitability and functional neuronal regeneration. The adsorption curve first increased and then fell with the increase of $\text{NH}_2\text{-GO}$ content; the peak was reached at 6 wt %. Combined with the SEM observation, it could be found that there were not enough active groups for adsorption at low content, as shown in Figure 4B, and the graphene network was too complicated at high concentration as shown in Figure 4D, which masked the groups and caused the opposite effect. The obvious network structure at a middle concentration proved its efficient adsorption ability, as shown in Figure 4C.

2.5. Morphological Characterization after $\text{NH}_2\text{-GO}$ Treatment. The different role of $\text{NH}_2\text{-GO}$ was investigated in PRCN and PRSN. Cell viabilities were separately detected by the CCK-8 assay (Figure 5) after the $\text{NH}_2\text{-GO}$ treatment (1– $100\text{ }\mu\text{g/mL}$) in PRCN and PRSN.

Images after $\text{NH}_2\text{-GO}$ treatment at 2 and $4\text{ }\mu\text{g/mL}$ are presented in Figure 5A. Bright-field images of the PRCN and PRSN, taken with an Olympus IX71 microscope (Olympus, Japan), are shown in Figure 5A. Axonal connection and growth is distinctly observed. In addition, no conspicuous cell death is observed. The image of dissolved $\text{NH}_2\text{-GO}$ in tridistilled water is shown in Figure 5B.

Cell viability has a marked increase in $2\text{ }\mu\text{g/mL}$ $\text{NH}_2\text{-GO}$ -treated PRCN ($n = 12$, $t = 3.93$, $p < 0.001$) compared with the control. No remarkable changes were observed in the cell

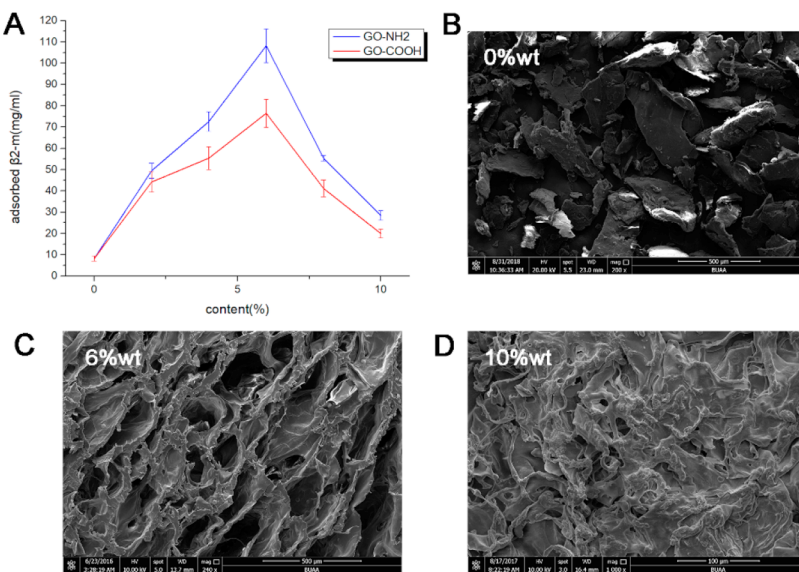


Figure 4. Adsorption curve and the surface view of different NH₂-GO content.

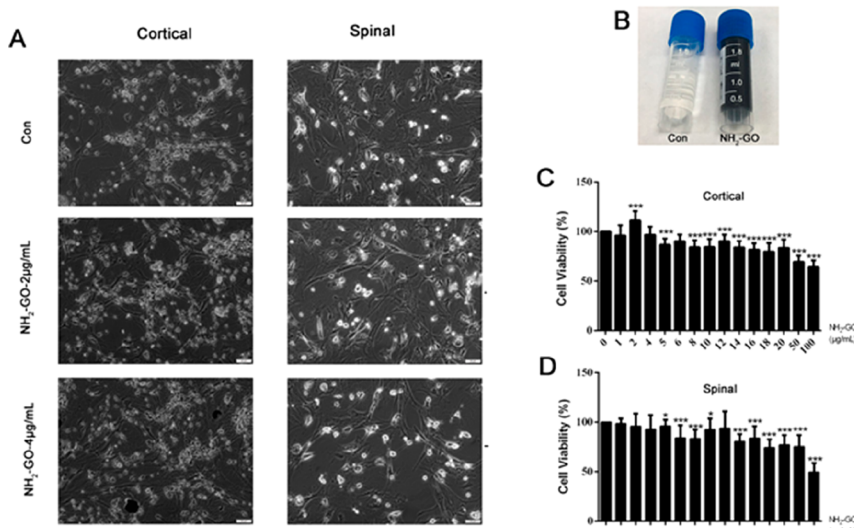


Figure 5. Effect of NH₂-GO on the neurite growth of PRCN and PRSN. (A) The bright field photos of PRCN (left panel) and PRSN (right panel) after NH₂-GO (2 and 4 μ g/mL) treatment, scale bars: 50 μ m. (B) Actual image of NH₂-GO in tridistilled water. (C) Cell viability was tested after NH₂-GO treatment (1–100 μ g/mL) in PRCN. (D) Cell growth in PRSN was tested by the CCK-8 assay after NH₂-GO treatment (1–100 μ g/mL). * p < 0.05, ** p < 0.01 and *** p < 0.001.

viability of PRCN after treatment with NH₂-GO at different concentrations (1, 4, and 6 μ g/mL). However, cell viability was significantly reduced ($n = 12$, $p < 0.001$) after treatment with NH₂-GO (5, 8, 10, 12, 14, 16, 18, 20, 50, and 100 μ g/mL) of PRCN. The results are shown in Figure 5C.

In the PRSN, NH₂-GO treatment cannot induce significant changes of cell survival at the concentration of 1, 2, 4, 5, and 12 μ g/mL. However, NH₂-GO at 6, 8, 10, 14, 16, 18, 20, 50, and 100 μ g/mL markedly inhibited the growth of cells growth ($n = 12$, $p < 0.05$) in PRSN. The results are presented in Figure 5D.

As the NH₂-GO concentration increased, cell viability decreased conspicuously both in PRCN and PRSN. When NH₂-GO concentration reached 14 μ g/mL, marked toxicity was observed. Thus, we selected NH₂-GO treatment at the concentration of 2 and 4 μ g/mL in this study.

Cell viability significantly increased in PRCN treated with NH₂-GO 2 μ g/mL; however, no conspicuous change in cell

viability was observed in PRSN after being treated with NH₂-GO at 2 μ g/mL. With an increase in NH₂-GO concentration, cell viability in both the cortical neurons and spinal cord neurons decreased significantly. The study showed that NH₂-GO at 2 μ g/mL was the proper concentration for neuronal growth. This may be related to the distinct structural properties of NH₂-GO such as enriched aminated-containing groups and high biocompatibility. Meanwhile, no studies on the side effect of NH₂-GO on neuronal viability have been reported; thus, graphene application can be considered for neural regeneration.

2.6. NH₂-GO Role on Neurite Outgrowth in PRCN and PRSN. In this study, PRCN and PRSN were stained with mouse anti- β Tubulin III antibody to detect the neuronal cytoskeleton. All nucleoli were dyed by DAPI. Merged images are also shown in the right of Figure 6A and Figure 7A.

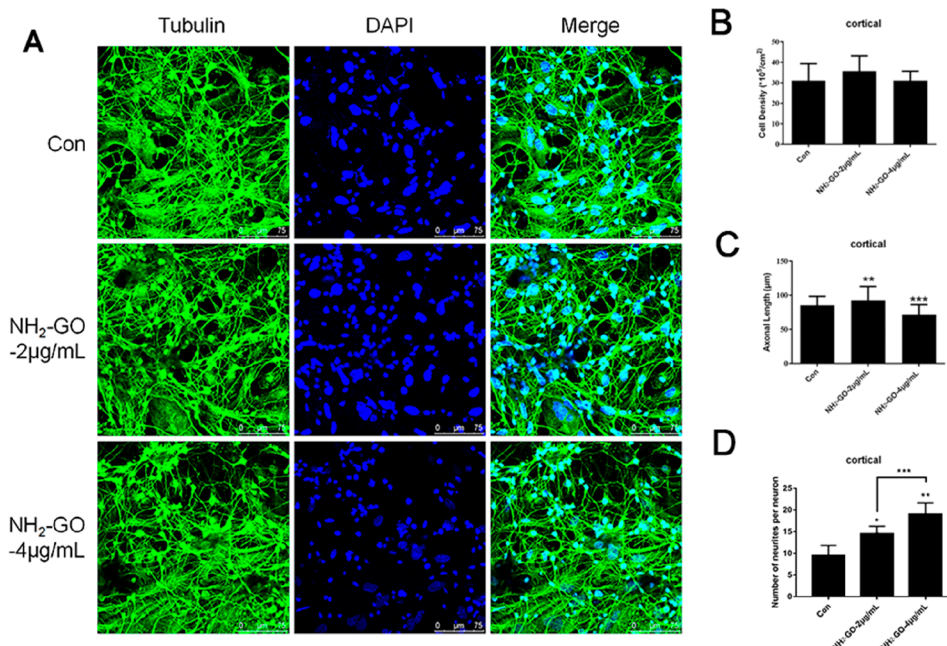


Figure 6. Role of NH₂-GO on the neuronal outgrowth in the PRCN. (A) Typical images of PRCN were stained with β -Tubulin III (left) and DAPI (middle), and the merged image (right). Scale bars: 75 μm . (B) No conspicuous difference of cell density was observed by NH₂-GO treatment. (C) Statistic analysis for axonal elongation after NH₂-GO treatment. (D) Statistic analysis for neurites branch number of per neuron. (* $p < 0.05$, ** $p < 0.01$ and *** $p < 0.001$).

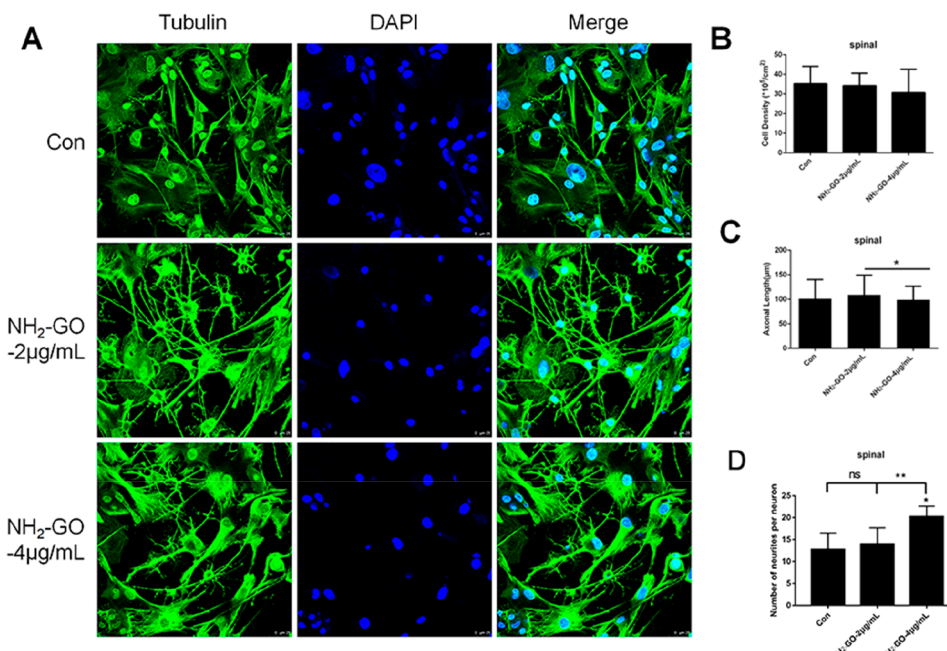


Figure 7. Effect of NH₂-GO on the neurite outgrowth in the PRSN. (A) Typical images of PRSN stained with β -Tubulin III (left) and DAPI (middle), and the merged image (right). Scale bars: 25 μm (B) No conspicuous difference of cell density were observed in NH₂-GO treated samples. (C) Statistic analysis for neurite elongation in NH₂-GO treated samples. (D) Statistic analysis for neurites branch numbers of per neuron. (* $p < 0.05$, ** $p < 0.01$).

In the PRCN, a concentration of NH₂-GO of 2 $\mu\text{g}/\text{mL}$ promoted neurite elongation ($n = 3$, $t = 3.10$, $p < 0.01$). Additionally, the neurite branch numbers per neuron have a significant increase in 2 and 4 $\mu\text{g}/\text{mL}$ ($n = 3$, $t = 4.095$, $p < 0.01$, $n = 3$, $t = 6.43$, $p < 0.001$), and the 4 $\mu\text{g}/\text{mL}$ group has a significant increase compared with the 2 $\mu\text{g}/\text{mL}$ group ($n = 3$, $t = 3.60$, $p < 0.01$). No marked changes of cell density occurred with NH₂-GO treatment, indicating NH₂-GO exerted no

neurotoxic effects on PRCN. The results are shown in Figure 6B–D.

In the PRSN, NH₂-GO cannot induce marked elongation of neurite except for the groups treated with NH₂-GO at 2 and 4 $\mu\text{g}/\text{mL}$. The group treated with NH₂-GO at 4 $\mu\text{g}/\text{mL}$ significantly decreased in axonal length relative to that of the group treated with NH₂-GO at 2 $\mu\text{g}/\text{mL}$ ($n = 3$, $t = 2.08$, $p < 0.05$). No conspicuous decrease in cell density was observed

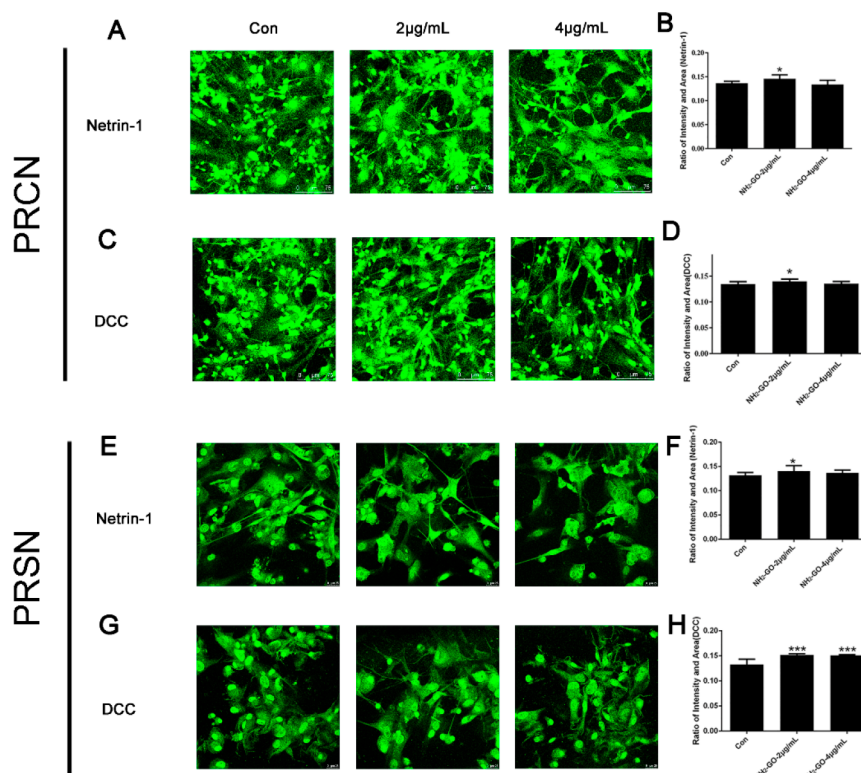


Figure 8. Netrin-1 and DCC expression in the NH₂-GO treated PRCN and PRSN. (A,C) Typical images of PRCN stained with Netrin-1 or DCC. Scale bars: 75 μ m. (B,D) Quantitative analysis of Netrin-1 and DCC by calculation the ratio of area and intensity in PRCN. (* $p < 0.05$). (E,G) Typical images of PRSN stained with Netrin-1 or DCC. Scale bars: 25 μ m. (F,H) Quantitative analysis of Netrin-1 and DCC by calculation of the ratio of area and intensity in PRSN (* $p < 0.05$, ** $p < 0.01$, *** $p < 0.001$).

after NH₂-GO treatment, suggesting that NH₂-GO exerted no neurotoxic effects on PRSN. Besides, the neurite branch numbers per neuron have a significant increase in the 4 μ g/mL group ($n = 3$, $t = 3.37$, $p < 0.05$), and the 4 μ g/mL group has a significant increase compared with the 2 μ g/mL group ($n = 3$, $t = 3.17$, $p < 0.01$). The results are shown in Figure 7B–D.

Axonal elongation significantly increased after NH₂-GO treatment at 2 μ g/mL in PRCN, but no conspicuous change was observed in spinal cord neurons. As NH₂-GO concentration increased, axonal elongation significantly decreased in PRSN and PRCN. However, both the cortical neurons and spinal cord neurons exhibited no significant change in cell density. Our study demonstrated that NH₂-GO at 2 μ g/mL exerts significant effects on axonal connective function. NH₂-GO may influence synapse formation during the axonal development. The aminated surface of graphene oxide has more positive ions in the culture cortical neurons, compared with the hydroxyl surface, and can alter the surface charges.¹²

2.7. NH₂-GO Activate Netrin-1/DCC in PRCN and PRSN. Netrin-1 binds to and activates DCC and can direct axon growth to target neurons; however, whether NH₂-GO activates neurite growth or not is not clear. To measure the expression of Netrin-1 and its receptor DCC in PRCN and PRSN, the neurons were immunostained to evaluate the intensity (Figure 8A,C,E,G).

NH₂-GO at 2 μ g/mL can induce a significant increase of both Netrin-1 and DCC in PRCN ($n = 7$, $p < 0.05$) (Figure 8B,D). In the PRSN, NH₂-GO at the concentration of 2 μ g/mL ($n = 7$, $t = 2.21$, $p < 0.05$) significantly increased Netrin-1 expression in PRSN as shown in the Figure 8F. NH₂-GO treatment at both 2 and 4 μ g/mL activated the DCC

expression (2 μ g/mL, $n = 7$, $t = 5.53$, $p < 0.001$; 4 μ g/mL, $n = 7$, $t = 5.32$, $p < 0.001$), and the result is shown in Figure 8H.

NH₂-GO treatment at 2 μ g/mL may significantly activate Netrin-1 and DCC, which influence neurite outgrowth in PRCN and PRSN.

2.8. Netrin-1 and DCC mRNA Level Analysis. In the NH₂-GO-treated PRCN and PRSN, all translated cDNA samples were subjected to real-time PCR assay. NH₂-GO at 2 μ g/mL could markedly increase Netrin-1 mRNA level ($n = 3$, $t = 3.69$, $p < 0.05$) and DCC mRNA level ($n = 3$, $t = 2.87$, $p < 0.05$) in PRCN (Figure 9A,B). However, no significant changes were observed in Netrin-1 and DCC mRNA level in PRSN (Figure 9C,D). These findings indicated that NH₂-GO of 2 μ g/mL has an influence on neurite outgrowth by upregulating the Netrin-1 and DCC mRNA level in the PRCN.

2.9. Netrin-1/DCC Expression Determined by NH₂-GO by Western Blot Assay. Different GO derivatives play an important role in neuronal development. Whether these GO oxide derivatives activate Netrin-1/DCC signaling to influence neurite outgrowth has yet to be determined. In this study, Netrin-1/DCC expression was determined by Western blots assay in the PRCN and PRSN after GO and COOH-GO (carboxylated graphene oxide) and NH₂-GO treatment.

In the PRCN, Netrin-1 expression was markedly increased ($n = 3$, $p < 0.05$) in GO-2 μ g/mL, COOH-GO-4 μ g/mL and NH₂-GO-2 μ g/mL treatments. In addition, DCC expression was also enhanced ($n = 3$, $p < 0.05$) by GO-2 μ g/mL and NH₂-GO-2 μ g/mL treatments. More interestingly, compared to the group treated with COOH-GO-4 μ g/mL, Netrin-1 expression increased more significantly in the NH₂-GO treated

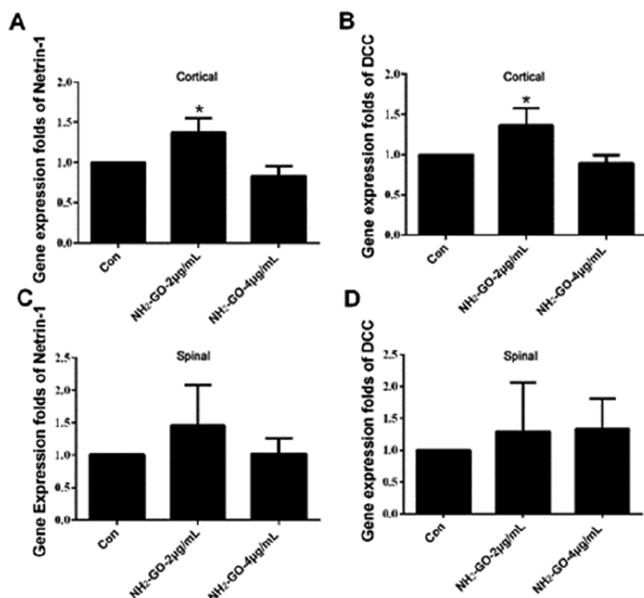


Figure 9. Real-time PCR assay results. NH₂-GO at 2 μg/mL activated mRNA level of Netrin-1 and DCC in PRCN (A, B), but no marked influence was detected in NH₂-GO treated PRSN (*p < 0.05).

PRCN (2 μg/mL, n = 3, t = 2.27, p < 0.05). Results are shown in Figure 10A–C.

In the PRSN, NH₂-GO treatment had a different effect on axonal guidance growth. Compared with the control, there are not any marked changes of Netrin-1 expression by GO, COOH-GO, and NH₂-GO treatments. There is a significant

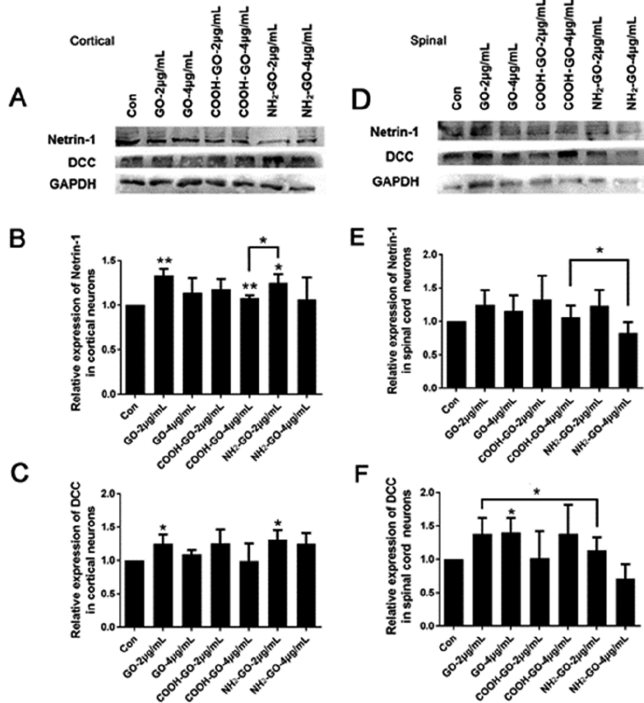


Figure 10. NH₂-GO role on Netrin-1 and DCC expression by Western blots assay. Protein bands were shown in PRCN (A) and PRSN (D) after NH₂-GO treatments. Histogram shows fold change of relative density of Netrin-1 and DCC (B, C, E, F). Average (three experiments) results from densitometry analysis with Netrin-1 and DCC normalized by GAPDH, respectively (*p < 0.05, **p < 0.01).

increase of DCC (n = 3, t = 3.20, p < 0.05) after GO (4 μg/mL) treatment, but Netrin-1 expression in PRSN was still unchanged (Figure 10D–F). Compared with the COOH-GO-4 μg/mL group, Netrin-1 expression was enhanced significantly by NH₂-GO 4 μg/mL treatment (n = 3, t = 4.60, p < 0.05) in PRSN. Moreover, compared with GO-2 μg/mL group, there is a conspicuous change of DCC expression by treatment with NH₂-GO-2 μg/mL (n = 3, t = 4.69, p < 0.05) in PRSN (Figure 10F).

These findings indicated that NH₂-GO-2 μg/mL could well activate Netrin-1/DCC signaling to promote neurite growth in PRCN.

2.10. RhoGTPase Signaling Involved the Neurite Outgrowth Triggered by NH₂-GO. RhoGTPase may play a role in the process of NH₂-GO influencing the axonal growth. NH₂-GO-treated neurons were then blocked by RhoA inhibitor C3 exoenzymes, and the protein bands are shown in Figure 11A. NH₂-GO treatment at 2 μg/mL led to marked

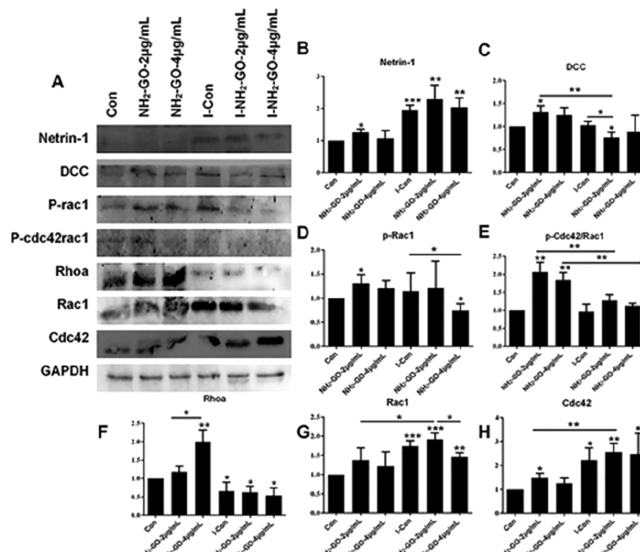


Figure 11. NH₂-GO activates RhoGTPase signaling. (A) Protein bands were detected by Western blot assay in NH₂-GO- and C3-exoenzyme-treated PRCN. (B–H) Histogram shows the difference of the relative density. Average (three experiments) results were calculated from densitometry analysis. Each protein expression level was normalized by GAPDH, respectively (*p < 0.05, **p < 0.01 and ***p < 0.001).

increases in Netrin-1 (2 μg/mL, n = 3, t = 4.293, p < 0.05) and DCC (2 μg/mL, n = 3, t = 3.499, p < 0.05) expression. When RhoA was inhibited by C3-Exo, Netrin-1 expression increased conspicuously after NH₂-GO treatment at 2 μg/mL (n = 3, p < 0.01). The results are shown in Figure 11B,C.

To confirm the roles of NH₂-GO, small RhoGTPase, and phosphorylated RhoGTPase (Cdc42, Rac1, RhoA, phosphorylated-Rac1, phosphorylated-Cdc42/Rac1), these signal molecules were evaluated by Western blot assay (Figure 11D–H). More interestingly, Cdc42 was significantly enhanced after NH₂-GO treatment at 2 μg/mL (n = 3, t = 4.17, p < 0.05) and increased considerably more after treatment with C3 exoenzymes (I-con, n = 3, t = 4.04, p < 0.05; 2 μg/mL, n = 3, t = 7.71, p < 0.01; 4 μg/mL, n = 3, t = 2.95, p < 0.05).

No marked changes of Rac1 occurred after NH₂-GO treatment, but when C3 exoenzymes blocked the role RhoA, Rac1 expression increased conspicuously after NH₂-GO

treatment (I-con, $n = 3$, $t = 8.91$, $p < 0.001$, 2 $\mu\text{g}/\text{mL}$, $n = 3$, $t = 9.56$, $p < 0.001$, 4 $\mu\text{g}/\text{mL}$, $n = 3$, $t = 7.12$, $p < 0.01$). Phosphorylated-Rac1 (P-Rac1) expression increased conspicuously after $\text{NH}_2\text{-GO}$ treatment (2 $\mu\text{g}/\text{mL}$, $n = 3$, $t = 3.06$, $p < 0.05$), and it was inhibited by C3 exoenzymes after $\text{NH}_2\text{-GO}$ treatment at 4 $\mu\text{g}/\text{mL}$ ($n = 3$, $t = 3.13$, $p < 0.05$).

Phosphorylated-Cdc42/Rac1(P-Cdc42/Rac1) expression increased conspicuously after $\text{NH}_2\text{-GO}$ treatment at 2 $\mu\text{g}/\text{mL}$ ($n = 3$, $t = 6.88$, $p < 0.001$) and 4 $\mu\text{g}/\text{mL}$ ($n = 3$, $t = 6.74$, $p < 0.01$), and P-Cdc42/Rac1 expression was inhibited by C3 exoenzymes after $\text{NH}_2\text{-GO}$ treatment at 2 $\mu\text{g}/\text{mL}$ ($n = 3$, $t = 2.91$, $p < 0.05$) and 4 $\mu\text{g}/\text{mL}$ ($n = 3$, $t = 3.10$, $p < 0.05$). Moreover, RhoA conspicuously increased after $\text{NH}_2\text{-GO}$ treatment at 4 $\mu\text{g}/\text{mL}$ ($n = 3$, $t = 5.43$, $p < 0.01$). However, RhoA expression decreased conspicuously after treatment with C3 exoenzymes and $\text{NH}_2\text{-GO}$ at 2 $\mu\text{g}/\text{mL}$ ($n = 3$, $t = 3.96$, $p < 0.05$) and 4 $\mu\text{g}/\text{mL}$ ($n = 3$, $t = 3.83$, $p < 0.05$).

Therefore, this study suggested that $\text{NH}_2\text{-GO}$ could influence the expression of Netrin-1/DCC and the downstream RhoGTPase to influence the growth of neurons.

In this study, $\text{NH}_2\text{-GO}$ treatment at 2 $\mu\text{g}/\text{mL}$ activated Netrin-1 and DCC. More interestingly, RhoGTPase (C3-Exo) inhibited the RhoA, but it activated Cdc42, Rac-1 in the cortical neurons treated with $\text{NH}_2\text{-GO}$. Thus, findings suggested that Netrin-1 is essential for activating axonal guidance growth after $\text{NH}_2\text{-GO}$ treatment, which was confirmed in a previous study.²⁷ Marsick indicated that Netrin-1 can promote actin polymerization by up-regulating the activity of the actin depolymerization factor (ADF)/cofilin (AC) family. As an important receptor for Netrin-1, DCC may also play an important role in this regulation system. In addition, a previous study indicated that the Netrin-1/DCC signaling pathway is involved in the axonal guidance to the growth cone.²⁸ Our study further confirmed that Netrin-1/DCC signaling may involve the guidance growth triggered by $\text{NH}_2\text{-GO}$ treatment.

3. METHODS

3.1. Ethics Statement. In this study, related animal tests are according to Provisions and General Recommendation of Chinese Experimental Animals Administration Legislation (Permit Number: SCXK (Beijing) 2006-0025). Animal care protocols were approved by the Animal Care Committee of Beihang University.

3.2. Synthesis of $\text{NH}_2\text{-GO}$. Aminated graphene oxide ($\text{NH}_2\text{-GO}$) has been synthesized according to the Hummers' method and then became aminated through a thermal shock method. A certain amount of natural graphite powder and NaNO_3 were mixed in suitable H_2SO_4 (98 wt %) and then stirred for 12 h below zero for deep oxidation. KMnO_4 and H_2O_2 were used in this process to control the oxidation. The mixture was filtered, and the solid was collected into distilled water. The material was separated from the mixture through differential centrifugation. Finally, we put the material back into the water again. The produced solution was added into 20 mL of ethylenediamine and then subjected to magnetic stirring in a 70 °C water bath for 12 h in a reactor after mixing.

The resulting solution was purified by centrifugation (3500 rpm, 15 min) three times. The product was finally dried by lyophilization, and $\text{NH}_2\text{-GO}$ was obtained.

3.3. Materials Characterization. **3.3.1. SEM.** A scanning electron microscope (SEM, FEI250, U.S.A.) was used to explore the surface morphology of the $\text{NH}_2\text{-GO}$ composite. The accelerated voltage was 10 kV. The average diameter of the structure was analyzed on the SEM Images Program.

3.3.2. Raman Spectroscopy. Raman spectroscopy was performed to verify the existence of amino in $\text{NH}_2\text{-GO}$. GO fabricated by

Hummers' method was also tested for comparison. The result was a curve with specific line widths, intensities, and Raman shifts. The curve was determined by the number of graphene layers, laser excitation energy, doping, and strain. The graphene oxide modified by chemical doping could be accurately determined by Raman spectroscopy. The equipment was worked in the range of 3000–500 cm^{-1} at 1.5 cm^{-1} resolution and averaging 100 scans.

3.3.3. Thermal Analysis. Thermal analysis was performed to test the thermal stability and composition of $\text{NH}_2\text{-GO}$ composite. Sample of $\text{NH}_2\text{-GO}$ composite (100 mg) or GO was tested in simultaneous thermal analyzer (ZCT-A, China) under nitrogen atmosphere protection. The temperature range was 30 °C ~ 530 °C, the heating rate was 10 °C/min.

3.3.4. Adsorption Performance. The adsorption performance measurement was carried out to evaluate the affinity of sundry active groups in $\text{NH}_2\text{-GO}$. Chitosan (CS) was incorporated as a support material, and carboxylated graphene oxide was selected as a reference material. $\beta 2\text{-m}$ was selected as a representative adsorbed target of a different size. The desired amount of the composite materials was added into the solution, which contained $\beta 2\text{-m}$ (50 mL, 0.5 mg/mL) in an Erlenmeyer flask. Then the Erlenmeyer flask was placed on the flat ST5 CAT shaker at 110 rpm and 37 °C. The Enzyme Labeled Instrument (Clario star, German BMG) was applied to confirm the concentration of the adsorbed target. The calibration curves of those targets were adjusted by plotting the absorbance against the known concentration of the solution, respectively. The characteristic peak of $\beta 2\text{-m}$ (λ_{max}) was taken at a wavelength of 540 nm nm in the UV region. Every 30 min, the absorbance of the solution was tested at λ_{max} . Finally, after reaching sorption equilibrium, the maximum detoxification quantity of the scaffold was calculated on the basis of the following equation:

$$q = \frac{(C_1 - C_2) \times V}{W}$$

q = amount of detoxified uremic toxins (mg/g);
 C_1 = initial concentration (mg/mL) of the toxin solution;
 C_2 = final concentration (mg/mL) of the toxin solution;
 V = volume of the toxin solution (mL);
 W = weight of the scaffold (g) used in the experiment.

3.4. Cell Culture. According to our previous methods, rat cortical neurons (PRCN) and spinal cord neurons (PRSN) were cultured in vitro.²⁹ Newborn SD rats were received from the laboratory animal center of Peking University.

Rat cortical and spinal cord neurons were dissected and separated respectively from the cortex and spinal cord at 4 °C. PRCN and PRSN were treated with 0.25% trypsin at 37 °C for 20 min. Then dispersed cells were seeded on the 6-well plates, 96-well plates, or 60 mm dishes at a concentration of 1×10^6 cells/mL (PRCN) and 5×10^5 cells/ml (PRSN). All cells were cultured in the Dulbecco's modified Eagles' medium (DMEM) with 20% newborn bovine serum at 37 °C with 95% air and 5% CO_2 . The cells were left to grow for 2 or 3 days, then adding cytosine arabinoside(4 $\mu\text{g}/\text{mL}$) to prevent the division and growth of glia cells. The culture medium was renewed every 3 days during the culture process.

3.5. Aminated Graphene Oxide ($\text{NH}_2\text{-GO}$) Treatment. $\text{NH}_2\text{-GO}$ plays a role on the neuronal outgrowth, but its precise mechanism is unknown. The nanoparticles of $\text{NH}_2\text{-GO}$ were suspended in the tridistilled water as a storage solution of 1 mg/mL. The $\text{NH}_2\text{-GO}$ solution was gradually diluted with DMEM at 0–100 $\mu\text{g}/\text{mL}$. Here, primary cultured neurons were treated by various $\text{NH}_2\text{-GO}$ treatments, respectively (0–100 $\mu\text{g}/\text{mL}$), in the third or fourth day after culture. The cells continued to be cultured for 3 days. Morphological changes of neuronal growth and survival after $\text{NH}_2\text{-GO}$ treatment were observed by a fluorescence microscope (IX71, Olympus, Japan).

3.6. Cell Viability Assay. Living cells were counted by a CCK-8 kit (Beyotime, China) according to previous methods.³⁵ The kit reagent was diluted with 91% DMEM, and then 110 μL of the diluted reagent was to the cells in each well after the cells were washed with DMEM. The cell were incubated at 37 °C for 2 h. The absorbance

was detected by the enzyme linked immunosorbent assay (ELISA) plate reader at 450 nm to measure the cell viability.

3.7. Immunofluorescence Staining. After aminated graphene ($\text{NH}_2\text{-GO}$) treatment, β -tubulin III, Netrin-1, and DCC were stained by immunofluorescence assay according to our previous methods.²⁵ Primary antibodies were diluted by PBS plus bovine serum albumin (BSA, 1%, 1:100) and incubated at 4 °C overnight, which were provided by Abcam, Cambridge, U.K. The secondary antibodies were FITC-conjugated antibodies (1:100, Zhongshan, Beijing, China) and were reacted for 60 min at room temperature. Nuclei were stained with 4'6-diamidino -2-phenylindole (DAPI, Sigma) for 3 min.

Cell imaging and photography were performed on a confocal microscope (Leica TCS SPE, Germany) by a 40× oil immersion objective. Cell density was determined by DAPI staining with a hemocytometer. The neurite length was measured with the LAS AF software (Leica, Germany). The axonal length was measured as the distance from the cell body to axonal terminal. The neurite branches (including dendrite and axon) per neuron were measured using ImageJ. All the samples were analyzed over 100 cells in 3 counts per experiment. Average (three experiments) results were calculated from morphological analysis. The fluorescence intensity was measured as levels of Netrin-1 and DCC expression by ImageJ. The cell area was determined by manually tracing the original fluorescence image. At least three samples from different locations were taken and analyzed.

3.8. Reverse Transcription-Polymerase Chain Reaction (RT-PCR) Analysis. Trizol (Invitrogen, Carlsbad, CA, U.S.A.) was used for RNA isolation from cultured cells. After the extraction of RNA, reverse transcription (RT) was performed with Takara reagent kit and 2 μg of RNA for each sample. Gene sequences were selected, respectively, from GenBank no. NM-053731, NM-007831, and NM-017008. Primers were as follows:

Rat Netrin-1,
S: 5'-TCCGATCCCAAGAAA GCG -3',
AS: 5'-GAGCGACAGAGTGAGCGTAA-3'.
Rat DCC,
S: 5'-TAAC CTGCTTGTCTATAACCG-3',
AS: 5'-TGAATGGGAGGCACTTTT-3'.
Rat GAPDH,
S: 5'-GGTGGTCCAGGGTTTCTTA-3',
AS: 5'-TTGTCTCCTGCGA CTTCA -3'.

Amplification was done (Step 1: 94 °C, 5 min; Step 2: 94 °C, 30 s; Step 3: 58 °C, 30 s; Step 4: 72 °C, 10 s; Step 5: back to Step 2 for 39 cycles; Step 6: 72 °C, 10 min) in an Eppendorf Mastercycler (Eppendorf, Hamburg, Germany), and the results were analyzed by a BioRad ChemiDoc XRS imaging system (BioRad, Hercules, CA, U.S.A.).

3.9. Western Blot. Protein samples were collected from the cultured neurons after $\text{NH}_2\text{-GO}$ treatment, and the concentrations were quantified by BCA kit (Pierce, Rockford, IL). Then all samples were subjected to SDS-PAGE and Western blot assay according to our previous methods.³⁰ Transferred PVDF membranes were incubated with primary antibodies for Netrin-1 (1:500, Abcam, U.S.A.), DCC (1:500, Abcam, U.S.A.), Rac1 (1:1000, Abcam, U.S.A.), Cdc42 (1:1000, Abcam, U.S.A.), RhoA (1:1000, Abcam, U.S.A.), and GAPDH (1:1000, Santa Cruz, CA) phosphorylated-Rac1 (1:1000, Abcam, U.S.A.), phosphorylated-Cdc42/Rac1 (1:1000, Abcam, U.S.A.) at 4 °C overnight. Horseradish peroxidase-conjugated secondary antibodies (1:3000) were incubated for 2 h. Finally, membranes were exposed, and images were captured using Universal Hood II (Bio-Rad, U.S.A.). The results were normalized to corresponding GAPDH bands.

3.10. Statistical Analysis. All experimental results data are expressed as mean \pm standard error means. To compare the differences between the two groups, a *t* test or a one-way analysis of variance was performed here. Statistical significance was at * $p < 0.05$, ** $p < 0.01$, and *** $p < 0.001$.

4. CONCLUSIONS

Graphene oxide derivatives are widely applied in the nervous tissue engineering. In the present study, $\text{NH}_2\text{-GO}$ is considerably more suitable for axonal guidance and growth, particularly in PRCN rather than in PRSN. $\text{NH}_2\text{-GO}$ possesses desirable electrical characteristics because the amino group in aminated graphene exhibits higher reactivity and can react with many other compounds, thereby improving the dispersibility of graphitization amination and strengthening the effect of composite material. Thus, $\text{NH}_2\text{-GO}$ promotes axonal elongation and activates Netrin-1/DCC signaling, RhoGTPase pathway is involved in the $\text{NH}_2\text{-GO}$ induced neurite outgrowth process in PRCN. It provides a new method for nerve regeneration.

■ AUTHOR INFORMATION

Corresponding Authors

Gang Zhou — Key Laboratory for Biomechanics and Mechanobiology of Ministry of Education, School of Biological Science and Medical Engineering, Beijing Advanced Innovation Centre for Biomedical Engineering, and Shenzhen Research Institute of Beihang University, Beihang University, Beijing 100083, China;  orcid.org/0000-0001-6887-4108; Phone: +86-10-82338755; Email: zhougang@buaa.edu.cn

Yubo Fan — Key Laboratory for Biomechanics and Mechanobiology of Ministry of Education, School of Biological Science and Medical Engineering, Beijing Advanced Innovation Centre for Biomedical Engineering, and Shenzhen Research Institute of Beihang University, Beihang University, Beijing 100083, China; National Research Center for Rehabilitation Technical Aids, Beijing 100176, China; Phone: +86-10-82339428; Email: yubofan@buaa.edu.cn; Fax: +86-10-82339428

Authors

Meili Liu — Key Laboratory for Biomechanics and Mechanobiology of Ministry of Education, School of Biological Science and Medical Engineering and Beijing Advanced Innovation Centre for Biomedical Engineering, Beihang University, Beijing 100083, China

Chongquan Huang — Key Laboratory for Biomechanics and Mechanobiology of Ministry of Education, School of Biological Science and Medical Engineering and Beijing Advanced Innovation Centre for Biomedical Engineering, Beihang University, Beijing 100083, China

Zhengtai Jia — Key Laboratory for Biomechanics and Mechanobiology of Ministry of Education, School of Biological Science and Medical Engineering and Beijing Advanced Innovation Centre for Biomedical Engineering, Beihang University, Beijing 100083, China

Zhijun Zhao — Key Laboratory for Biomechanics and Mechanobiology of Ministry of Education, School of Biological Science and Medical Engineering and Beijing Advanced Innovation Centre for Biomedical Engineering, Beihang University, Beijing 100083, China

Xiongfuxiao — Key Laboratory for Biomechanics and Mechanobiology of Ministry of Education, School of Biological Science and Medical Engineering and Beijing Advanced Innovation Centre for Biomedical Engineering, Beihang University, Beijing 100083, China

Anqing Wang — Key Laboratory for Biomechanics and Mechanobiology of Ministry of Education, School of Biological Science and Medical Engineering and Beijing Advanced

Innovation Centre for Biomedical Engineering, Beihang University, Beijing 100083, China

Ping Li – Key Laboratory for Biomechanics and Mechanobiology of Ministry of Education, School of Biological Science and Medical Engineering and Beijing Advanced Innovation Centre for Biomedical Engineering, Beihang University, Beijing 100083, China

Xiali Guan – Key Laboratory for Biomechanics and Mechanobiology of Ministry of Education, School of Biological Science and Medical Engineering and Beijing Advanced Innovation Centre for Biomedical Engineering, Beihang University, Beijing 100083, China

Complete contact information is available at:

<https://pubs.acs.org/10.1021/acschemneuro.9b00625>

Author Contributions

M.L. conducted the cell experiments and wrote and revised the manuscript. C.H. cultured the cells and was involved in the manuscript revision. Z.J. performed the Western blot assay. A.W. performed the PCR assay. X.X. prepared the materials and performed the materials' characterization. X.G. prepared the submitting materials. L.P. conducted the materials' treatment experiment. G.Z. and Y.F. conceived the overall idea and designed the experiments. All the images used in this manuscript were originally created by our authors from original data.

Notes

The authors declare no competing financial interest.

ACKNOWLEDGMENTS

This study was supported by funds from the National Natural Science Foundation of China (NSFC) Research Grant (31971238, 81970900, 11421202, 61227902, 51574246, 61871014, 11827803, 31771019), and National key research and development program (2016YFC1100704, 2016YFC1102203, 2017YFC0108505), the Fundamental Research Funds for the Central Universities (No. YWF-19-BJ-J-203), Science, Technology and Innovation Commission of Shenzhen Municipality (No. JCYJ20180307123641888).

REFERENCES

- (1) Lu, P., Woodruff, G., Wang, Y., Graham, L., Hunt, M., Wu, D., Boehle, E., Ahmad, R., Poplawski, G., Brock, J., Goldstein, L. S., and Tuszynski, M. H. (2014) Long-distance axonal growth from human induced pluripotent stem cells after spinal cord injury. *Neuron* 83 (4), 789–796.
- (2) Lancaster, M. A., Corsini, N. S., Wolfinger, S., Gustafson, E. H., Phillips, A. W., Burkard, T. R., Otani, T., Livesey, F. J., and Knoblich, J. A. (2017) Guided self-organization and cortical plate formation in human brain organoids. *Nat. Biotechnol.* 35 (7), 659–666.
- (3) Fatehullah, A., Tan, S. H., and Barker, N. (2016) Organoids as an in vitro model of human development and disease. *Nat. Cell Biol.* 18 (3), 246–254.
- (4) Min, K.J., Kim, T.H., and Choi, J.W. (2017) Magnetic Force-Driven Graphene Patterns to Direct Synaptogenesis of Human Neuronal Cells. *Materials* 10 (10), 1151.
- (5) Okur, Z., Senturk, O. I., Yilmaz, C., Gulseren, G., Mammadov, B., Guler, M. O., and Tekinay, A. B. (2018) Promotion of neurite outgrowth by rationally designed NGF-beta binding peptide nanofibers. *Biomater. Sci.* 6 (7), 1777–1790.
- (6) Zhu, Y. W., Murali, S., Cai, W. W., Li, X. S., Suk, J. W., Potts, J. R., and Ruoff, R. S. (2010) Graphene and Graphene Oxide: Synthesis, Properties, and Applications. *Adv. Mater.* 22 (35), 3906–3924.
- (7) Zhu, X. B., Cui, Y. M., Chang, X. J., and Wang, H. (2016) Selective solid-phase extraction and analysis of trace-level Cr(III), Fe(III), Pb(II), and Mn(II) Ions in wastewater using diethylenetriamine-functionalized carbon nanotubes dispersed in graphene oxide colloids. *Talanta* 146, 358–363.
- (8) Park, S. Y., Park, J., Sim, S. H., Sung, M. G., Kim, K. S., Hong, B. H., and Hong, S. (2011) Enhanced differentiation of human neural stem cells into neurons on graphene. *Adv. Mater.* 23 (36), H263–267.
- (9) Li, N., Zhang, Q., Gao, S., Song, Q., Huang, R., Wang, L., Liu, L., Dai, J., Tang, M., and Cheng, G. (2013) Three-dimensional graphene foam as a biocompatible and conductive scaffold for neural stem cells. *Sci. Rep.* 3 (1), 1604–1604.
- (10) Ma, Q., Yang, L., Jiang, Z., Song, Q., Xiao, M., Zhang, D., Ma, X., Wen, T., and Cheng, G. (2016) Three-Dimensional Stiff Graphene Scaffold on Neural Stem Cells Behavior. *ACS Appl. Mater. Interfaces* 8 (50), 34227–34233.
- (11) Solanki, A., Chueng, S. T., Yin, P. T., Kappera, R., Chhowalla, M., and Lee, K. B. (2013) Axonal alignment and enhanced neuronal differentiation of neural stem cells on graphene-nanoparticle hybrid structures. *Adv. Mater.* 25 (38), 5477–5482.
- (12) Alegret, N., Criado, A., and Prato, M. (2017) Recent Advances of Graphene-based Hybrids with Magnetic Nanoparticles for Biomedical Applications. *Curr. Med. Chem.* 24 (5), 529–536.
- (13) Chen, Y., Xie, B., Ren, Y., Yu, M., Qu, Y., Xie, T., Zhang, Y., and Wu, Y. (2014) Designed nitrogen doping of few-layer graphene functionalized by selective oxygenic groups. *Nanoscale Res. Lett.* 9 (1), 646–646.
- (14) Feng, L. Z., Zhang, S. A., and Liu, Z. A. (2011) Graphene based gene transfection. *Nanoscale* 3 (3), 1252–1257.
- (15) Kostarelos, K., Vincent, M., Hebert, C., and Garrido, J.A. (2017) Graphene in the Design and Engineering of Next-Generation Neural Interfaces. *Adv. Mater.* 29 (42), 1700909.
- (16) Convertino, D., Luin, S., Marchetti, L., and Coletti, C. (2018) Peripheral Neuron Survival and Outgrowth on Graphene. *Front. Neurosci.* 12, 1.
- (17) Kang, E. S., Kim, D. S., Suhito, I. R., Choo, S. S., Kim, S. J., Song, I., and Kim, T. H. (2017) Guiding osteogenesis of mesenchymal stem cells using carbon-based nanomaterials. *Nano convergence* 4 (1), 2–2.
- (18) Sperry, R. W. (1963) Chemoaffinity in the Orderly Growth of Nerve Fiber Patterns and Connections. *Proc. Natl. Acad. Sci. U. S. A.* 50 (4), 703–710.
- (19) O’Leary, D. D. (1994) Developmental neurobiology-Attractive guides for axons. *Nature* 371 (6492), 15–16.
- (20) Drescher, U. (1996) Netrins find their receptor. *Nature* 384 (6608), 416–417.
- (21) Sun, K. L. W., Correia, J. P., and Kennedy, T. E. (2011) Netrins: versatile extracellular cues with diverse functions. *Development* 138 (11), 2153–2169.
- (22) Ly, A., Nikolaev, A., Suresh, G., Zheng, Y., Tessier-Lavigne, M., and Stein, E. (2008) DSCAM is a netrin receptor that collaborates with DCC in mediating turning responses to netrin-1. *Cell* 133 (7), 1241–1254.
- (23) Tu, T., Zhang, C., Yan, H., Luo, Y., Kong, R., Wen, P., Ye, Z., Chen, J., Feng, J., Liu, F., Wu, J. Y., and Yan, X. (2015) CD146 acts as a novel receptor for netrin-1 in promoting angiogenesis and vascular development. *Cell Res.* 25 (3), 275–287.
- (24) Ke, X., Li, Q., Xu, L., Zhang, Y., Li, D., Ma, J., and Mao, X. (2015) Netrin-1 overexpression in bone marrow mesenchymal stem cells promotes functional recovery in a rat model of peripheral nerve injury. *J. Biomed. Res.* 29 (5), 380–389.
- (25) Liu, M., Jia, Z., Xiao, X., Zhang, Z., Li, P., Zhou, G., and Fan, Y. (2018) Carboxylated graphene oxide promoted axonal guidance growth by activating Netrin-1/deleted in colorectal cancer signaling in rat primary cultured cortical neurons. *J. Biomed. Mater. Res., Part A* 106 (6), 1500–1510.
- (26) Palejwala, A. H., Fridley, J. S., Mata, J. A., Samuel, E. L., Luerssen, T. G., Perlaky, L., Kent, T. A., Tour, J. M., and Jea, A. (2016) Biocompatibility of reduced graphene oxide nanoscaffolds

following acute spinal cord injury in rats. *Surg. Neurol. Int.* 7 (1), 75–75.

(27) Marsick, B. M., Flynn, K. C., Santiago-Medina, M., Bamburg, J. R., and Letourneau, P. C. (2010) Activation of ADF/Cofilin Mediates Attractive Growth Cone Turning Toward Nerve Growth Factor and Netrin-1. *Dev. Neurobiol.* 70 (8), 565–588.

(28) Ren, X. R., Ming, G. L., Xie, Y., Hong, Y., Sun, D. M., Zhao, Z. Q., Feng, Z., Wang, Q., Shim, S., Chen, Z. F., Song, H. J., Mei, L., and Xiong, W. C. (2004) Focal adhesion kinase in netrin-1 signaling. *Nat. Neurosci.* 7 (11), 1204–1212.

(29) Liu, M., Zhou, G., Song, W., Li, P., Liu, H., Niu, X., and Fan, Y. (2012) Effect of nano-hydroxyapatite on the axonal guidance growth of rat cortical neurons. *Nanoscale* 4 (10), 3201–3207.

(30) Liu, M., Niu, X., Zhou, G., Jia, Z., Li, P., and Fan, Y. (2018) Potential effect of mechano growth factor E-domain peptide on axonal guidance growth in primary cultured cortical neurons of rats. *J. Tissue Eng. Regener. Med.* 12 (1), 70–79.